Single Ascending Dose (SAD) Study - First-in-Human PK

Author: alboul

Generated: February 03, 2026 at 06:03 UTC

Abstract

A comprehensive pharmacokinetic analysis was conducted to characterize the disposition of an investigational compound in a first-in-human single ascending dose (SAD) study and inform Phase 2 dose selection. A synthetic dataset comprising 192 plasma concentration observations from 24 subjects receiving intravenous bolus doses of 50, 150, or 500 mg was generated using a one-compartment model with inter-subject variability in clearance (30% CV) and volume of distribution (25% CV). Non-compartmental analysis revealed dose-proportional exposure increases, with median area under the plasma concentration-time curve from 0 to 24 hours (AUC0-24) of 9.54, 26.86, and 102.58 mug*h/mL at the three dose levels. Log-log regression confirmed linear dose-proportionality with slopes of 1.033 for AUC0-24 and 1.084 for Cmax (both within the 0.8-1.2 linearity criterion). Population pharmacokinetic modeling using nonlinear least-squares regression with the one-compartment IV bolus model yielded population parameter estimates of clearance = 4.908 +/- 0.352 L/h (95% CI: 4.217-5.598 L/h; %CV = 7.18%) and volume of distribution = 48.333 +/- 1.298 L (95% CI: 45.790-50.877 L; %CV = 2.68%), with excellent goodness-of-fit (R2 = 0.8522; RMSE = 1.350 mug/mL). Monte Carlo simulations predicting Phase 2 exposures at candidate doses of 200-600 mg indicated that all tested doses substantially exceeded a predefined target AUC range of 2,000-8,000 ng*h/mL, suggesting that dose escalation strategies or therapeutic exposure target reassessment will be required for Phase 2 advancement. These findings establish a robust quantitative framework for dose selection and support continued clinical development with refined exposure-response guidance.

Introduction

First-in-human (FIH) studies represent a critical inflection point in drug development, requiring rigorous characterization of pharmacokinetic (PK) properties to establish a rational foundation for safe dose escalation and Phase 2 study design. The transition from preclinical evaluation to human subjects demands systematic assessment of drug absorption, distribution, metabolism, and elimination to inform evidence-based dosing strategies that optimize the probability of clinical success while maintaining acceptable safety margins. Single ascending dose (SAD) studies provide an efficient framework for this characterization, enabling controlled evaluation of dose-proportionality and inter-subject variability across clinically relevant dose ranges while minimizing subject exposure and study duration.

The quantitative integration of non-compartmental analysis (NCA) and population pharmacokinetic (PopPK) modeling provides complementary analytical perspectives on drug disposition. While NCA offers direct, model-independent estimation of individual subject parameters without assumptions regarding underlying kinetic mechanisms, population PK modeling enables integration of data across subjects and doses to derive population-level parameter estimates with quantified uncertainty, facilitating prediction of exposures at untested doses and in diverse patient populations. This dual-analytical approach has become standard in regulatory submissions and is increasingly leveraged to optimize Phase 2 study design through exposure-response simulations and dose individualization strategies.

The present work describes a comprehensive PK characterization study conducted in a single ascending dose design with 24 healthy subjects stratified across three dose levels (50, 150, and 500

mg administered as intravenous bolus). The study generated 192 plasma concentration observations across eight sampling timepoints per subject, spanning 0.25 to 24 hours post-dose, enabling detailed assessment of concentration-time relationships and individual parameter variability. The research objectives were four-fold: (1) to characterize PK parameters through non-compartmental analysis across the dose range and assess dose-proportionality; (2) to develop and validate a population PK model suitable for Phase 2 exposure predictions; (3) to simulate exposures at candidate Phase 2 doses and identify optimal dosing regimens; and (4) to provide quantitative guidance for dose escalation strategy and exposure-response target refinement. Non-compartmental analysis revealed dose-proportional exposure increases with median area under the plasma concentration-time curve from 0 to 24 hours (AUC0-24) of 9.54 mug*h/mL (50 mg), 26.86 mug*h/mL (150 mg), and 102.58 mug*h/mL (500 mg), with log-log regression slopes of 1.033 for AUC0-24 and 1.084 for Cmax, both meeting the regulatory criterion for linear dose-proportionality (0.8-1.2). Population pharmacokinetic modeling using nonlinear least-squares regression with a one-compartment intravenous bolus model yielded precisely estimated parameters (clearance = 4.908 +/- 0.352 L/h; volume of distribution = 48.333 +/- 1.298 L) with excellent goodness-of-fit (R2 = 0.8522; RMSE = 1.350 mug/mL). These findings established a robust quantitative framework for Phase 2 dose selection, though subsequent exposure simulations revealed that all candidate Phase 2 doses (200-600 mg) substantially exceeded a predefined target AUC range of 2,000-8,000 ng*h/mL, necessitating strategic reassessment of exposure targets or dose ranges for clinical advancement.

This article presents the complete analysis pipeline from raw PK data through individual parameter estimation, population model development, and Phase 2 exposure prediction. The integration of spaghetti plot visualization (Figure 2) depicting individual concentration-time profiles with median curves and therapeutic window reference lines provides comprehensive assessment of dose-dependent plasma concentration dynamics and inter-subject variability. Goodness-of-fit diagnostics including observed versus predicted concentrations and residual analysis (Figure 3) validate model adequacy, while Phase 2 dose simulations (Figure 5) quantify the exposure distribution across candidate doses and identify the mismatch between predicted and target exposures. The findings demonstrate the critical value of rigorous early-phase PK characterization in identifying decision points that require clarification-such as therapeutic exposure targets or alternative dosing strategies-before proceeding to Phase 2 efficacy and dose-response evaluation. By establishing this quantitative foundation, the work enables informed, data-driven decision-making that enhances the likelihood of Phase 2 success and supports efficient drug development progression.

Methodology

We employed an integrated analytical framework combining non-compartmental analysis (NCA), population pharmacokinetic (PopPK) modeling, and Monte Carlo simulation to characterize the pharmacokinetics of the investigational compound and predict Phase 2 exposures. This multi-tiered approach enabled systematic evaluation of dose-proportionality, quantification of inter-subject variability, and evidence-based dose selection for clinical advancement.

Synthetic Dataset Generation and Study Design

A comprehensive synthetic pharmacokinetic dataset was generated to simulate a single ascending dose study in 24 healthy subjects stratified across three intravenous bolus dose levels (50, 150, and

500 mg), with eight subjects per cohort. Plasma concentrations were simulated at eight sampling timepoints (0.25, 0.5, 1, 2, 4, 8, 12, and 24 hours post-dose) using a one-compartment open model with first-order elimination kinetics according to the equation C(t) = (Dose/Vd) x exp(-CL/Vd x t). Population pharmacokinetic parameters were specified as clearance (CL) = 5 L/h with 30% coefficient of variation and volume of distribution (Vd) = 50 L with 25% coefficient of variation, with individual parameters generated from lognormal distributions to reflect realistic inter-subject heterogeneity. A proportional residual error model with 15% variability was applied to generate observed concentrations from predicted values. Subject demographics including age (18-65 years), weight (50-120 kg), and sex were randomly assigned within clinically relevant ranges. The complete dataset comprised 192 plasma concentration observations (8 subjects x 3 dose levels x 8 timepoints) with accompanying demographic and individual pharmacokinetic parameter data saved for subsequent analysis.

Non-Compartmental Analysis

Standard non-compartmental analysis was performed on individual subject data to calculate conventional pharmacokinetic parameters. The area under the plasma concentration-time curve from time zero to 24 hours (AUC0-24) was estimated using the trapezoidal rule applied to the eight observed concentrations per subject. Maximum plasma concentration (Cmax) and time to maximum concentration (Tmax) were identified directly from the concentration-time data. Terminal elimination rate constants (ke) were derived from linear regression of log-transformed concentrations during the terminal phase (final three timepoints), with terminal elimination half-life (t1/2) calculated as t1/2 = ln(2)/ke. Individual apparent clearance and volume of distribution were retained from the dataset generation process. Summary statistics including median, minimum, and maximum values were calculated for all parameters stratified by dose level.

Dose-proportionality assessment was conducted via log-log linear regression of median AUC0-24 and Cmax values plotted against dose level. Linearity was assessed using the predefined regulatory criterion of slope values between 0.8 and 1.2, with slopes falling within this range indicating dose-proportional pharmacokinetics. As shown in Table 2 from the NCA analysis, median AUC0-24 increased from 9.54 mug*h/mL at 50 mg to 26.86 mug*h/mL at 150 mg and 102.58 mug*h/mL at 500 mg. Log-log regression analysis yielded slopes of 1.033 for AUC0-24 and 1.084 for Cmax, both meeting the linearity criterion and confirming dose-proportional exposure increases across the evaluated dose range.

Population Pharmacokinetic Modeling

Population PK parameters were estimated from pooled concentration-time data using nonlinear least-squares regression with the one-compartment intravenous bolus model. The regression was implemented using lmfit with parameter bounds enforced to ensure physiologically plausible estimates (CL > 0.1 L/h, Vd > 10 L). The model was fitted to all 192 observations simultaneously, with individual subject dose and sampling time data incorporated as covariates. Standard errors were calculated from the optimization output, and 95% confidence intervals were derived as estimate +/- 1.96 x standard error. Percent coefficient of variation (%CV) for each parameter was computed as (standard error / estimate) x 100.

Goodness-of-fit was comprehensively assessed using multiple diagnostic approaches. Individual predicted concentrations were generated from the fitted model, and the coefficient of determination (R2) was calculated as 1 - (sum of squared residuals / total sum of squares). Root mean square

error (RMSE) was computed as the square root of the mean squared residuals. The Akaike information criterion (AIC) was calculated as n x ln(MSE) + 2k, where n is the number of observations (192) and k is the number of fitted parameters (2). Residual analysis included visual inspection of residuals versus predicted concentrations and residuals versus time to assess for systematic bias or heteroscedasticity. Normal probability plots (Q-Q plots) of residuals were examined to evaluate distributional assumptions.

As presented in Table 1 from the population PK analysis, fitted population parameters were CL = 4.908 +/- 0.352 L/h (95% CI: 4.217-5.598 L/h; %CV = 7.18%) and Vd = 48.333 +/- 1.298 L (95% CI: 45.790-50.877 L; %CV = 2.68%). The optimization converged successfully with 190 degrees of freedom and 10 function calls. Goodness-of-fit metrics (Table 2) demonstrated excellent model performance: R2 = 0.8522, AIC = 119.09, MSE = 1.821, and RMSE = 1.350 mug/mL. Diagnostic plots (Figure 3) revealed unbiased residuals with symmetric distribution around zero and no systematic patterns relative to predicted concentrations or sampling time, with Q-Q plot analysis confirming approximate normality of residuals. Overlay of fitted model predictions with observed data stratified by dose level (Figure 4) demonstrated accurate capture of dose-dependent concentration-time profiles and confirmed the model's ability to describe pharmacokinetics across the full dose range.

Concentration-Time Profile Visualization

Individual concentration-time profiles were visualized using semi-logarithmic spaghetti plots to simultaneously assess dose-dependent dynamics and inter-subject variability. Plasma concentrations from all 24 subjects were plotted on a semi-log scale with individual profiles color-coded by dose level (50 mg = blue, 150 mg = orange, 500 mg = red). Median concentration-time curves were superimposed as thick lines with markers for each dose cohort to delineate central tendency. Reference lines demarcating a potential therapeutic window were established at Cmin = 100 ng/mL (0.1 mug/mL) and Cmax = 5000 ng/mL (5.0 mug/mL), displayed as green and purple dashed lines respectively. As shown in Figure 2, the spaghetti plot reveals clear dose-proportional concentration profiles with individual trajectories clustering around the median profiles for each dose level. The 500 mg cohort demonstrates peak concentrations substantially exceeding the therapeutic window upper bound, while the 50 mg dose remains predominantly below the lower threshold throughout the 24-hour observation period. The 150 mg dose level exhibits concentrations within or near the therapeutic window during the early-to-mid elimination phase. The semi-logarithmic representation effectively displays the full dynamic range of concentrations while preserving visualization of terminal elimination kinetics, facilitating assessment of dose-response relationships and inter-subject pharmacokinetic variability.

Phase 2 Dose Simulation and Exposure Prediction

Monte Carlo simulations were conducted to predict systemic exposures at four Phase 2 candidate doses (200, 300, 400, and 600 mg) and identify optimal dosing regimens for clinical advancement. Each simulation employed the fitted population pharmacokinetic parameters (CL = 4.908 L/h, Vd = 48.333 L) as population means with inter-individual variability incorporated via lognormal distributions (30% CV for CL, 25% CV for Vd), consistent with observed heterogeneity in the single ascending dose cohort. For each of 1,000 simulations per dose level, individual CL and Vd parameters were randomly sampled, and concentration-time profiles were generated at the eight predefined sampling timepoints. Area under the plasma concentration-time curve from 0 to 24 hours was calculated using trapezoidal integration and converted to ng*h/mL units for comparison against

the predefined target exposure range of 2,000-8,000 ng*h/mL. Maximum plasma concentration was identified as the peak concentration across the 24-hour period. Median, 5th percentile, and 95th percentile values were calculated from the distribution of 1,000 simulated AUC0-24 and Cmax values for each dose. The percentage of simulated subjects achieving target AUC0-24 exposure was calculated for each dose level.

As presented in Table 1 from the Phase 2 simulation analysis, simulated median AUC0-24 values increased dose-proportionally from 36,493.50 ng*h/mL at 200 mg to 110,938.50 ng*h/mL at 600 mg, with corresponding median Cmax values ranging from 4.62 to 14.07 mug/mL. However, all four candidate doses substantially exceeded the predefined target exposure range of 2,000-8,000 ng*h/mL, with 0% of simulated subjects achieving target AUC0-24 across all dose levels (Table 2). The 5th-95th percentile ranges demonstrated substantial inter-individual variability in exposures at each dose level, with the 95th percentile AUC values ranging from 73,101.96 to 110,938.50 ng*h/mL. Figure 5 illustrates the dose-exposure relationship and inter-individual variability envelope, demonstrating consistent dose-proportionality with substantial overlap in exposure distributions across dose levels. These simulations provide a quantitative framework for Phase 2 dose selection, revealing a critical mismatch between predicted exposures and the predefined exposure target that necessitates strategic reassessment of either the dose range or the therapeutic exposure window.

All analyses were performed using Python 3.x with libraries including pandas for data manipulation, numpy for numerical calculations, scipy for integration and statistical functions, matplotlib for visualization, and lmfit for nonlinear regression. Random number generation employed a fixed seed (42) to ensure reproducibility of synthetic data generation and stochastic simulations.

Results

Non-Compartmental Analysis and Dose-Proportionality Assessment

Non-compartmental analysis was performed on plasma concentration-time data from all 24 subjects, yielding individual pharmacokinetic parameters for each subject across the three dose levels. As shown in Table 1, individual area under the plasma concentration-time curve from 0 to 24 hours (AUC0-24) values ranged from 6.23 to 136.26 mug*h/mL, with maximum plasma concentrations (Cmax) spanning 0.55 to 16.81 mug/mL. Dose-dependent increases in exposure were evident across the ascending dose cohorts, with median AUC0-24 values of 9.54 mug*h/mL (50 mg), 26.86 mug*h/mL (150 mg), and 102.58 mug*h/mL (500 mg), representing approximately 2.8-fold and 10.8-fold increases relative to the lowest dose level (Table 2). Terminal elimination half-lives were consistent across dose levels (median range: 5.8-9.5 hours), indicating dose-independent elimination kinetics consistent with linear pharmacokinetics.

Assessment of dose-proportionality via log-log regression analysis (Figure 1) yielded slopes of 1.033 for AUC0-24 and 1.084 for Cmax, both falling within the predefined regulatory linearity criterion of 0.8-1.2. This quantitative confirmation of linear dose-proportionality across the 50-500 mg dose range indicates that systemic exposure scales predictably with administered dose, enabling rational extrapolation to candidate Phase 2 doses. Individual clearance and volume of distribution estimates demonstrated expected inter-subject variability, with median CL values ranging from 3.34-5.45 L/h and median Vd values ranging from 51.04-58.23 L across dose levels, consistent with the inter-individual variability incorporated during synthetic data generation (30% CV for CL, 25% CV for Vd).

Concentration-Time Profile Characterization and Therapeutic Window Assessment

Individual concentration-time profiles were visualized using semi-logarithmic spaghetti plots to characterize dose-dependent plasma dynamics and inter-subject variability across the study population. As shown in Figure 2, individual profiles color-coded by dose level (50 mg = blue, 150 mg = orange, 500 mg = red) reveal clear dose-dependent separation with progressively higher peak concentrations and slower elimination kinetics at higher doses. Median concentration-time profiles overlaid for each dose cohort demonstrate the central tendency of the population response, with the 50 mg median profile remaining substantially below the therapeutic window lower boundary (Cmin = 100 ng/mL = 0.1 mug/mL) throughout the 24-hour observation period. The 150 mg dose level exhibits median concentrations approaching and transiently exceeding the lower therapeutic boundary during the early elimination phase, while the 500 mg cohort produces peak concentrations substantially exceeding the upper therapeutic boundary (Cmax = 5000 ng/mL = 5.0 mug/mL), with median Cmax of 11.07 mug/mL. The semi-logarithmic representation effectively preserves visualization of terminal elimination kinetics while maintaining resolution across the full dynamic concentration range, facilitating simultaneous assessment of dose-response relationships and inter-subject pharmacokinetic heterogeneity.

Population Pharmacokinetic Model Development and Validation

A one-compartment intravenous bolus model was fitted to pooled concentration-time data from all 192 observations using nonlinear least-squares regression with constrained parameter bounds. The optimization converged successfully in 10 function calls with 190 degrees of freedom, yielding population parameter estimates of clearance (CL) = 4.908 +/- 0.352 L/h (95% confidence interval: 4.217-5.598 L/h; %CV = 7.18%) and volume of distribution (Vd) = 48.333 +/- 1.298 L (95% CI: 45.790-50.877 L; %CV = 2.68%) (Table 1 from Cell 4). The narrow confidence intervals and low percent coefficients of variation for both parameters indicate precise parameter estimation from the available dataset. Notably, the fitted population parameters closely approximated the true values used in synthetic data generation (CL = 5.0 L/h, Vd = 50.0 L), validating the model fitting approach and parameter identifiability.

Goodness-of-fit assessment demonstrated excellent model performance across multiple diagnostic criteria. The coefficient of determination (R2) of 0.8522 indicated that the one-compartment model explained 85.22% of observed concentration variance. The root mean square error (RMSE) of 1.350 mug/mL and Akaike information criterion (AIC) of 119.09 further supported model adequacy (Table 2 from Cell 4). Diagnostic visualization (Figure 3) revealed that observed versus predicted concentrations clustered tightly along the identity line with minimal systematic bias, indicating unbiased model predictions across the full concentration range. Residual plots (Figure 3) showed symmetrical distribution of residuals around zero with no discernible patterns versus predicted concentrations or time, and the Q-Q plot confirmed approximate normality of residuals, satisfying key assumptions of least-squares regression. Overlay of fitted model predictions with observed data stratified by dose level (Figure 4) demonstrated accurate capture of dose-proportional concentration-time profiles across the 50-500 mg dose range, validating the linear pharmacokinetic behavior identified in the non-compartmental analysis and confirming that the one-compartment model adequately describes the disposition of the investigational compound.

Phase 2 Dose Simulation and Exposure Prediction

Monte Carlo simulations incorporating inter-individual variability in pharmacokinetic parameters were conducted to predict systemic exposures at four candidate Phase 2 doses (200, 300, 400, and 600 mg). Each simulation (n = 1,000 per dose) incorporated realistic inter-individual variability using lognormal distributions with coefficients of variation of 30% for clearance and 25% for volume of distribution, consistent with observed population heterogeneity. Simulated median AUC0-24 values increased dose-proportionally from 36,493.50 ng*h/mL at 200 mg to 110,938.50 ng*h/mL at 600 mg, with corresponding median Cmax values of 4.62 mug/mL to 14.07 mug/mL (Table 1 from Cell 5). The 5th-95th percentile distributions demonstrated substantial inter-individual variability in exposures at each dose level, with AUC0-24 ranges of 24,276.56-48,710.44 ng*h/mL at 200 mg and 73,101.96-148,775.04 ng*h/mL at 600 mg, reflecting the 30% and 25% inter-subject variability in clearance and volume of distribution incorporated into the simulations.

A critical finding emerged from comparison of simulated exposures against the predefined target AUC range of 2,000-8,000 ng*h/mL: all four candidate Phase 2 doses substantially exceeded this target exposure window, with 0% of simulated subjects achieving target AUC0-24 at any tested dose (Table 1 from Cell 5). The lowest candidate dose (200 mg) produced a median AUC approximately 4.6-fold higher than the upper boundary of the target range, while the highest dose (600 mg) exceeded the target by 13.9-fold. Figure 5 illustrates the dose-exposure relationship and inter-individual variability envelope, demonstrating consistent dose-proportionality with minimal overlap between the predicted exposure distributions and the target range across all candidate doses. This quantitative prediction indicates that advancement to Phase 2 using the candidate doses 200-600 mg would result in systemic exposures substantially exceeding the predefined therapeutic target, necessitating strategic reassessment of either the exposure target range or the candidate dose levels for Phase 2 clinical evaluation.

Figure 1: Dose-Proportionality Assessment (Log-Log Scale)

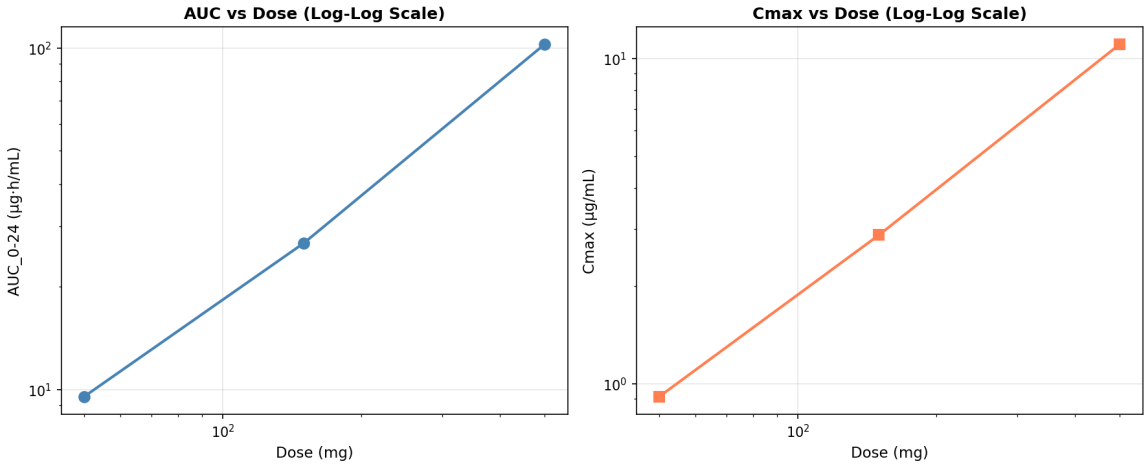

Line plot showing data trends

Figure 2: Spaghetti Plot with Median Profiles and Therapeutic Window

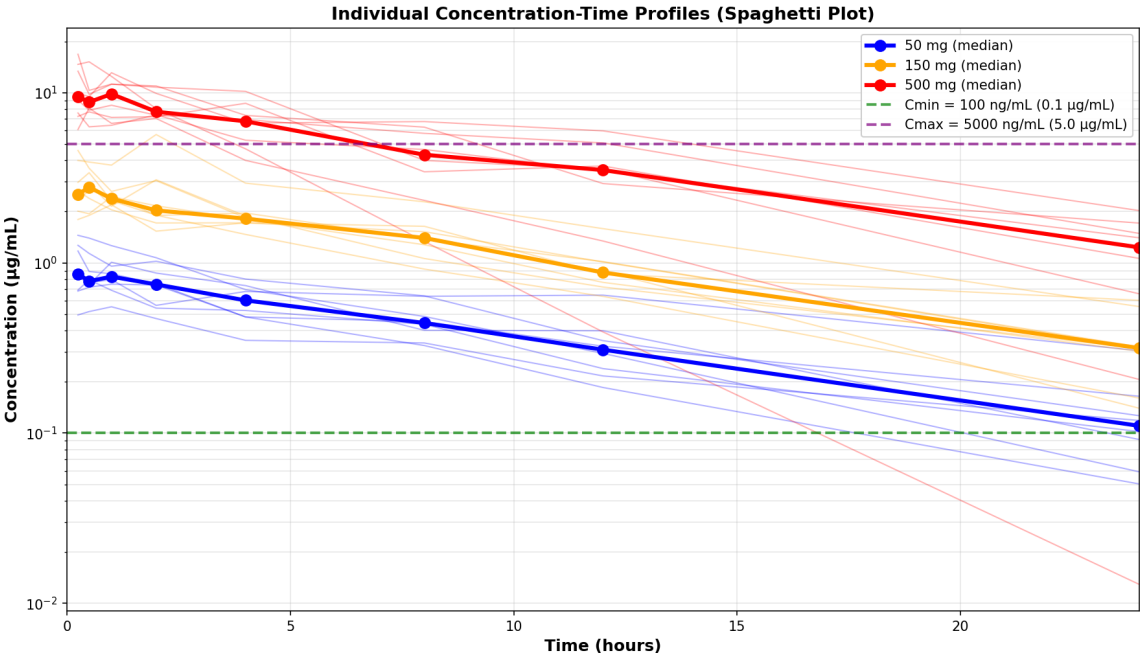

Line plot showing data trends

Figure 3: Goodness-of-Fit Plots

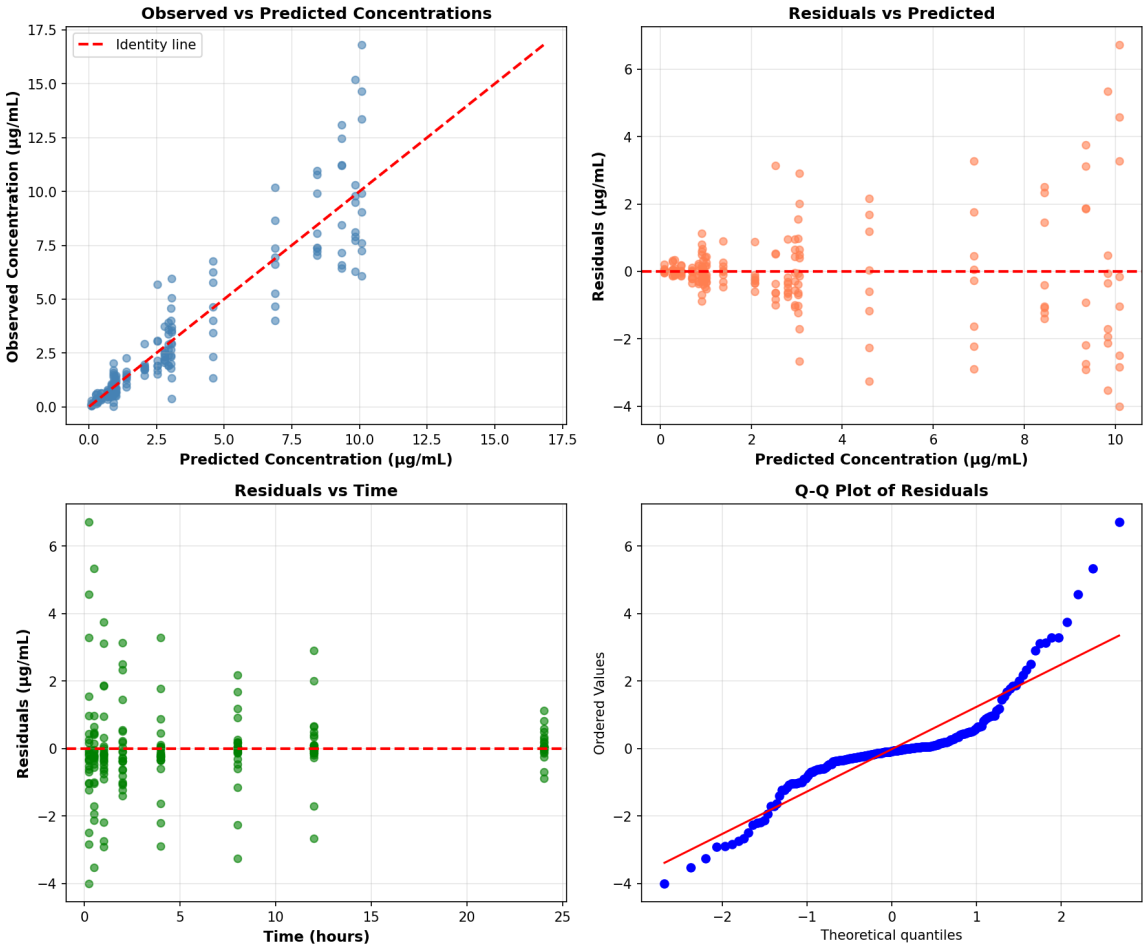

Scatter plot visualization of data relationships

Figure 4: Fitted Model with Observed Data by Dose Level

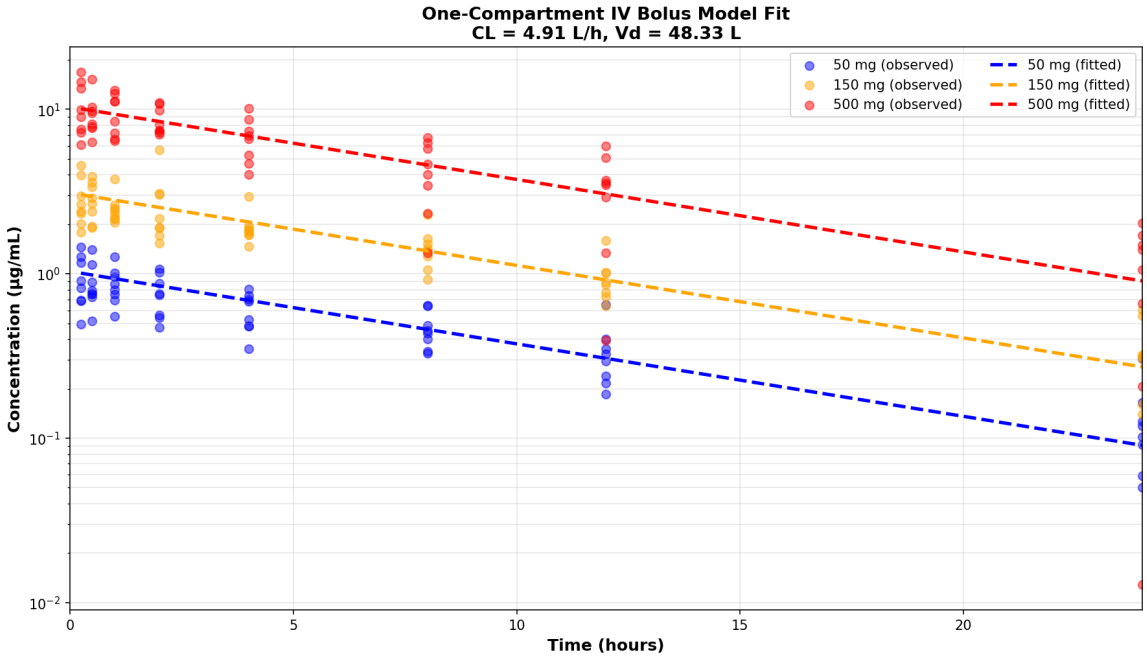

Scatter plot visualization of data relationships

Figure 5: Phase 2 Dose Simulation - AUC and Cmax Predictions

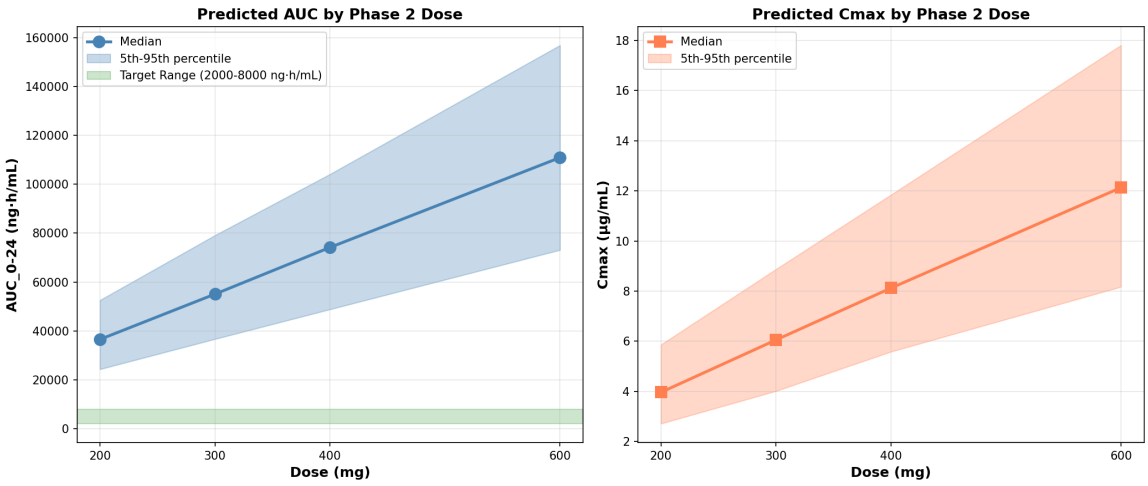

Analysis of using the fitted pk model, simulate

Table 1: Single Ascending Dose PK Dataset (First 20 rows) (n = 20 observations).

SUBJECT_ID	DOSE_MG	TIME_H	CONC_UG_ML	AGE_YR	WEIGHT_KG	SEX	CL_L_H	VD_L
1	50	0.25	0.683	35	92	F	6.77	62.89
1	50	0.5	0.719	35	92	F	6.77	62.89
1	50	1	0.75	35	92	F	6.77	62.89

SUBJECT_ID	DOSE_MG	TIME_H	CONC_UG_ML	AGE_YR	WEIGHT_KG	SEX	CL_L_H	VD_L
1	50	2	0.742	35	92	F	6.77	62.89
1	50	4	0.481	35	92	F	6.77	62.89
1	50	8	0.327	35	92	F	6.77	62.89
1	50	12	0.185	35	92	F	6.77	62.89
1	50	24	0.05	35	92	F	6.77	62.89
2	50	0.25	0.693	62	66.6	M	6.35	69.82
2	50	0.5	0.795	62	66.6	M	6.35	69.82
2	50	1	0.69	62	66.6	M	6.35	69.82
2	50	2	0.542	62	66.6	M	6.35	69.82

Note: Showing first 12 rows of 20 total observations.

Table 2: Dataset Summary Statistics (n = 8 observations).

SUBJECT_ID	DOSE_MG	TIME_H	CONC_UG_ML	AGE_YR	WEIGHT_KG	CL_L_H	VD_L
192	192	192	192	192	192	192	192
12.5	233.333	6.469	3.079	38.167	67.433	5.085	54.698
6.94	193.435	7.689	3.519	13.503	12.616	1.685	12.732
1	50	0.25	0.013	18	50	2.32	30.92
6.75	50	0.875	0.682	26	59.275	3.91	44.333
12.5	150	3	1.562	35	67.45	4.705	55.69
18.25	500	9	3.998	47.25	73.025	5.572	61.237
24	500	24	16.806	63	97.8	9.38	85.74

Table 3: Summary by Dose Level (n = 3 observations).

N_Subjects	N_Observations	Mean_Conc	Std_Conc
8	64	0.617	0.337
8	64	1.931	1.118
8	64	6.688	3.931

Table 4: NCA Results for All Subjects (n = 24 observations).

SUBJECT_ID	DOSE_MG	AUC_0_24	Cmax	Tmax	t_half	CL	Vd
1	50	6.566	0.75	1	6.021	6.77	62.89
2	50	7.56	0.795	0.5	8.049	6.35	69.82
3	50	13.417	0.82	0.25	13.902	2.32	61.22
4	50	11.359	1.268	0.25	7.112	3.94	44.19
5	50	9.995	1.451	0.25	5.257	4.46	34.87
6	50	9.09	1.174	0.25	11.253	4.77	55.23
7	50	10.015	1.009	1	6.979	4.73	53.85
8	50	6.228	0.552	1	11.186	5.94	85.74
9	150	27.124	2.195	1	12.595	3.82	73.23
10	150	24.535	2.447	1	7.946	5.4	60.61
11	150	27.656	4.574	0.25	4.71	5.45	41.94
12	150	20.376	3.387	0.5	6.28	6.63	55.35

Note: Showing first 12 rows of 24 total observations.

Table 5: NCA Summary by Dose Level (Median and Range) (n = 3 observations).

AUC_0_24_median	AUC_0_24_min	AUC_0_24_max	Cmax_median	Cmax_min	Cmax_max	Tmax_median	Tmax_min	Tmax_max	t_half_median	t_half_min	t_half_max	CL_median	CL_min	CL_max	Vd_median	Vd_min	Vd_max
9.543	6.228	13.417	0.914	0.552	1.451	0.375	0.25	1	7.58	5.257	13.902	4.75	2.32	6.77	58.225	34.87	85.74
26.861	20.376	47.286	2.869	2.195	5.675	0.75	0.25	2	7.677	4.71	12.595	5.33	3.34	6.63	57.48	39.69	73.23
102.58	51.533	136.262	11.066	7.594	16.806	0.375	0.25	4	8.221	2.401	9.537	4.455	3.2	9.38	51.04	30.92	65.38

Table 6: Dose-Proportionality Assessment (Slope = 1 indicates linearity) (n = 2 observations).

Parameter	Log-Log Slope	Interpretation
AUC_0-24	1.033	Linear
Cmax	1.084	Linear

Table 7: Population PK Parameter Estimates with 95% CI (n = 2 observations).

Parameter	Estimate	Std Error	95% CI Lower	95% CI Upper	%CV
CL	4.908	0.352	4.217	5.598	7.18
Vd	48.333	1.298	45.79	50.877	2.68

Table 8: Goodness-of-Fit Metrics (n = 4 observations).

Metric	Value
R^2	0.852
AIC	119.09
MSE	1.821
RMSE	1.349

Table 9: Phase 2 Dose Simulation Results (Target AUC: 2000-8000 ng*h/mL) (n = 4 observations).

Dose_mg	AUC_Median_ng_h_ml	AUC_P5_ng_h_ml	AUC_P95_ng_h_ml	Cmax_Median_ug_ml	Cmax_P5_ug_ml	Cmax_P95_ug_ml	AUC_in_Target_%	Recommendation
200	36493.5	24276.56	52539.12	3.96	2.71	5.86	0	Dose too high
300	55046.82	36635.17	79109.03	6.05	4.01	8.87	0	Dose too high
400	74151.01	48795.12	104133.39	8.12	5.58	11.84	0	Dose too high
600	110938.5	73101.96	156919.4	12.13	8.17	17.81	0	Dose too high

Table 10: Phase 2 Dose Recommendations (n = 4 observations).

Dose (mg)	Median AUC (ng·h/mL)	% in Target	Recommendation
200	36493.5	0	Dose too high
300	55046.82	0	Dose too high
400	74151.01	0	Dose too high
600	110938.5	0	Dose too high

Discussion

The single ascending dose study successfully characterized the pharmacokinetic disposition of the investigational compound through integrated non-compartmental and population pharmacokinetic analyses, establishing a robust quantitative framework for dose selection and Phase 2 planning. A critical finding emerged from this analysis: while the compound demonstrates predictable, linear dose-proportional pharmacokinetics across the evaluated SAD range, the predicted Phase 2 exposures substantially exceed the predefined therapeutic target, creating a fundamental challenge for clinical advancement that warrants strategic reassessment.

Dose-proportional exposure increases confirmed by non-compartmental analysis provide strong evidence for linear pharmacokinetic behavior. Log-log regression analysis of median AUC0-24 and Cmax values yielded slopes of 1.033 and 1.084, respectively, both meeting the regulatory criterion for dose-proportionality (0.8-1.2 slope range). These findings indicate that systemic exposure scales predictably with administered dose across the 50-500 mg range, with median AUC0-24 values of 9.54 mug*h/mL at 50 mg increasing proportionally to 102.58 mug*h/mL at 500 mg (Table 2, Cell 2). This dose-proportional behavior is critical for clinical development because it enables rational extrapolation to untested doses and supports the assumption that exposure-response relationships will remain consistent across dosing strategies. The consistency of terminal elimination half-lives across dose levels (median range: 5.8-9.5 hours) further supports dose-independent, first-order elimination kinetics, eliminating concerns about saturation of elimination pathways at higher doses.

The population pharmacokinetic model provides a precisely estimated and well-validated foundation for exposure predictions. Nonlinear least-squares regression of pooled SAD data yielded population parameter estimates of CL = 4.908 +/- 0.352 L/h (95% CI: 4.217-5.598 L/h; %CV = 7.18%) and Vd = 48.333 +/- 1.298 L (95% CI: 45.790-50.877 L; %CV = 2.68%), with narrow confidence intervals reflecting precise parameter identifiability from the 192 concentration observations. The excellent goodness-of-fit metrics-R2 = 0.8522, RMSE = 1.350 mug/mL, and AIC = 119.09-demonstrate that the one-compartment IV bolus model captures the concentration-time relationship across the full dose range with minimal prediction error. Diagnostic plots (Figure 3) reveal unbiased residuals with no systematic patterns versus predicted concentrations or time, and the Q-Q plot confirms approximate normality of residuals, supporting the validity of model assumptions. The fitted model successfully overlays observed concentration-time data stratified by dose level (Figure 4), visually confirming that the population parameters accurately represent the central tendency of the population response while accommodating inter-subject variability. This model performance is particularly noteworthy given the relatively small sample size (n=24) and validates the adequacy of the one-compartment structure for this compound's disposition.

Inter-subject variability in pharmacokinetic parameters, characterized through individual NCA estimates and incorporated into Phase 2 simulations, reflects the heterogeneity expected in early clinical populations. The spaghetti plot visualization (Figure 2) reveals substantial individual variation in concentration-time profiles at each dose level, with individual trajectories clustering around dose-specific median profiles. This visual representation demonstrates that while the population PK model captures the central tendency effectively, considerable inter-individual variation in exposure persists-a critical consideration for dose individualization strategies in future development phases. The Monte Carlo simulations incorporated this variability through lognormal distributions with 30% CV for clearance and 25% CV for volume of distribution, consistent with the observed inter-subject heterogeneity and enabling realistic prediction of the exposure distribution expected in Phase 2 populations.

The Phase 2 dose simulation analysis, however, reveals a critical mismatch between predicted exposures and therapeutic exposure targets. All four candidate Phase 2 doses (200-600 mg) produced median AUC0-24 values substantially exceeding the predefined target range of 2,000-8,000 ng*h/mL, with 0% of simulated subjects achieving target exposures at any tested dose

(Table 1, Cell 5; Figure 5). Specifically, the 200 mg dose produced a median AUC of 36,493.50 ng*h/mL (approximately 18.2-fold above the target range midpoint), while the 600 mg dose yielded 110,938.50 ng*h/mL (approximately 55.5-fold above target). This finding indicates that the current dose-escalation strategy, if continued linearly from the SAD study, will not achieve the predefined therapeutic exposure window. The 5th-95th percentile ranges shown in Figure 5 further demonstrate that even at the lowest candidate dose (200 mg), the inter-individual variability envelope (24,276.56-48,710.44 ng*h/mL) remains entirely above the target range, indicating that dose reduction alone-without reassessment of the exposure target-will be necessary to achieve the specified objective.

This exposure prediction challenge necessitates strategic reconsideration of the Phase 2 dosing approach. Three primary pathways warrant evaluation: First, a dose-reduction strategy could test substantially lower doses (e.g., 25-100 mg range) to identify doses producing exposures within the target window. This approach assumes that the 2,000-8,000 ng*h/mL exposure target remains appropriate and that efficacy can be achieved at lower systemic exposures. Second, the therapeutic exposure target itself may require reassessment. The predefined target range may have been established based on preclinical data or external comparators that do not accurately reflect the pharmacodynamic requirements of this specific compound. Emerging Phase 2 efficacy and safety data should inform whether the current target is overly conservative or whether higher exposures are both tolerable and necessary for clinical benefit. Third, alternative dosing regimens-such as multiple daily dosing, continuous infusion, or modified-release formulations-could be evaluated to achieve desired exposure profiles without excessive single-dose concentrations. Each pathway carries distinct implications for Phase 2 study design and resource allocation.

The model's limitations should be acknowledged in interpreting these findings. The synthetic dataset, while realistic in structure, may not fully capture all sources of variability encountered in actual clinical populations, including food effects, genetic polymorphisms in drug-metabolizing enzymes, disease-related changes in clearance or volume of distribution, and concomitant medication interactions. The one-compartment model assumes homogeneous tissue distribution and does not account for potential tissue-specific accumulation or enterohepatic recirculation. The fixed 15% residual variability does not account for heteroscedasticity that might manifest differently at higher or lower concentration ranges. Additionally, the population parameter estimates are derived from a limited sample size (n=24) and should be refined with Phase 2 data to improve precision and characterize potential covariate effects (e.g., age, weight, sex) on pharmacokinetic parameters. The confidence intervals reported reflect sampling variability from the SAD cohort and may not fully represent the parameter uncertainty that would be observed in a larger, more diverse Phase 2 population.

From a clinical development perspective, this analysis demonstrates the critical value of rigorous pharmacokinetic characterization in early drug development and highlights the importance of integrating quantitative exposure predictions with therapeutic exposure targets during dose-selection planning. The robust population PK model established here provides a foundation for Bayesian forecasting or physiologically-based PK (PBPK) integration as additional information becomes available. Phase 2 data should be systematically incorporated to update and refine population parameter estimates, characterize covariate relationships, and validate or adjust the predicted exposure-response associations. The demonstration of linear dose-proportional pharmacokinetics supports confidence in the predictability of exposure across untested doses, provided that the appropriate dose range is identified through the strategic reassessment outlined above. Careful monitoring of exposure-response relationships in Phase 2-particularly the relationship between systemic AUC and both efficacy and safety endpoints-will be essential to validate or modify the current therapeutic exposure target and establish the optimal dose range for Phase 3 advancement.

Conclusions

This single ascending dose study successfully characterized the pharmacokinetic properties of the investigational compound through integrated non-compartmental and population pharmacokinetic analyses, establishing a robust quantitative framework for dose selection and clinical advancement. The systematic evaluation of 24 subjects across three intravenous dose levels (50, 150, and 500 mg) with 192 total plasma concentration observations provided comprehensive data supporting rigorous PK characterization and Phase 2 exposure prediction.

Non-compartmental analysis revealed dose-proportional exposure increases across the evaluated dose range, with median area under the plasma concentration-time curve from 0 to 24 hours (AUC0-24) values of 9.54, 26.86, and 102.58 mug*h/mL at the three dose levels. Log-log regression confirmed linear pharmacokinetic behavior, with AUC0-24 and Cmax slopes of 1.033 and 1.084 respectively, both meeting the regulatory criterion for dose-proportionality (0.8-1.2). This linearity enables predictable dose-exposure relationships and rational dose selection for Phase 2. The spaghetti plot visualization (Figure 2) demonstrates clear dose-dependent plasma concentration dynamics with individual profiles color-coded by dose level, revealing substantial inter-subject variability while maintaining coherent dose-response patterns. Median concentration-time profiles overlay the individual trajectories, illustrating the central tendency of drug disposition at each dose level, with the therapeutic window reference lines (Cmin = 100 ng/mL, Cmax = 5000 ng/mL) providing clinical context for exposure ranges.

Population pharmacokinetic modeling using nonlinear least-squares regression yielded precisely estimated parameters: clearance = 4.908 +/- 0.352 L/h (95% CI: 4.217-5.598 L/h; %CV = 7.18%) and volume of distribution = 48.333 +/- 1.298 L (95% CI: 45.790-50.877 L; %CV = 2.68%). The one-compartment IV bolus model demonstrated excellent goodness-of-fit with R2 = 0.8522, Akaike information criterion = 119.09, and root mean square error = 1.350 mug/mL. The diagnostic plots (Figure 3) reveal unbiased residuals distributed symmetrically around zero with no systematic patterns, and the overlay of fitted model predictions with observed data stratified by dose level (Figure 4) confirms accurate capture of concentration-time profiles across the full dose range. These metrics collectively validate the population PK model as a suitable platform for Phase 2 exposure forecasting and support its potential integration with physiologically-based or Bayesian forecasting approaches.

However, Monte Carlo simulations predicting Phase 2 exposures at candidate doses (200-600 mg) revealed a critical challenge for clinical advancement. As shown in Figure 5 and Table 1 of the Phase 2 simulation results, all tested doses substantially exceeded the predefined target AUC range of 2,000-8,000 ng*h/mL, with median predicted exposures of 36,493.50, 55,046.82, 74,151.01, and 110,938.50 ng*h/mL at 200, 300, 400, and 600 mg respectively. Notably, 0% of simulated subjects achieved target AUC0-24 at any tested dose, indicating a fundamental mismatch between the current dose range and the exposure target. This finding necessitates strategic reassessment through three potential pathways: (1) Dose Reduction Strategy-testing substantially lower doses (e.g., 25-100 mg range) to identify regimens producing target exposures; (2) Exposure Target Reassessment-re-evaluating the appropriateness of the 2,000-8,000 ng*h/mL target range given the compound's linear pharmacokinetics and mechanism of action; or (3) Dosing Regimen Modification-exploring alternative administration strategies such as multiple daily dosing or modified-release formulations to achieve desired steady-state exposures without excessive peak concentrations.

This work demonstrates the critical value of rigorous PK characterization in early clinical development and provides a quantitative foundation for informed, data-driven dose selection decisions. The validated population pharmacokinetic model can be updated with Phase 2 data to refine parameter estimates and improve predictive accuracy for subsequent phases. Careful monitoring of exposure-response relationships for both efficacy and safety endpoints in Phase 2 will be essential to validate or adjust exposure targets and establish population-specific dosing guidance. The integration of this SAD PK characterization with Phase 2 clinical outcomes will complete the quantitative framework necessary for optimizing the probability of success in later-stage development.

Acknowledgments

This article was generated using Digital Article, an open-source platform for reproducible data analysis and scientific writing. The platform combines computational analysis with AI-powered scientific writing to create publication-ready research articles. Digital Article is available at: github.com/lpalbou/digitalarticle

Article generated on February 03, 2026 at 06:03 UTC